# ACS Energy LETTERS

# Unraveling the Role of Lithium in Enhancing the Hydrogen Evolution Activity of MoS$_2$: Intercalation versus Adsorption

Longfei Wu,[†] Nelson Y. Dzade,[‡,§] Miao Yu,[†] Brahim Mezari,[†] Arno J. F. van Hoof,[†] Heiner Friedrich,[⊥] Nora H. de Leeuw,[‡,§] Emiel J. M. Hensen,[†] and Jan P. Hofmann*,[†]

[†]Laboratory for Inorganic Materials and Catalysis, Department of Chemical Engineering and Chemistry, Eindhoven University of Technology, P.O. Box 513, 5600 MB Eindhoven, The Netherlands

[‡]Faculty of Geosciences, Utrecht University, Princetonlaan 8A, 3584 CB Utrecht, The Netherlands

[§]School of Chemistry, Cardiff University, Main Building, Park Place, CF10 3AT Cardiff, United Kingdom

[⊥]Laboratory of Materials and Interface Chemistry, Department of Chemical Engineering and Chemistry, Eindhoven University of Technology, P.O. Box 513, 5600 MB Eindhoven, The Netherlands

**S** *Supporting Information*

**ABSTRACT:** Molybdenum disulfide (MoS$_2$) is a highly promising catalyst for the hydrogen evolution reaction (HER) to realize large-scale artificial photosynthesis. The metallic 1T′-MoS$_2$ phase, which is stabilized via the adsorption or intercalation of small molecules or cations such as Li, shows exceptionally high HER activity, comparable to that of noble metals, but the effect of cation adsorption on HER performance has not yet been resolved. Here we investigate in detail the effect of Li adsorption and intercalation on the proton reduction properties of MoS$_2$. By combining spectroscopy methods (infrared of adsorbed NO, $^7$Li solid-state nuclear magnetic resonance, and X-ray photoemission and absorption) with catalytic activity measurements and theoretical modeling, we infer that the enhanced HER performance of Li$_x$MoS$_2$ is predominantly due to the catalytic promotion of edge sites by Li.
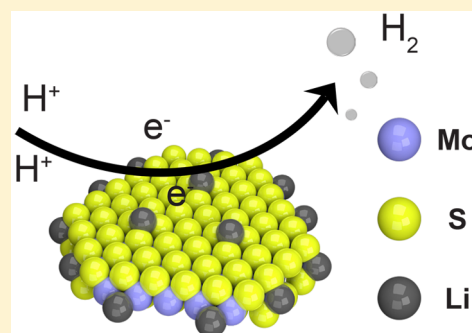
Molybdenum disulfide (MoS$_2$) has demonstrated significant potential to replace noble-metal-based catalysts in electrochemical hydrogen production. Like other transition-metal dichalcogenides (TMDs), MoS$_2$ can exist in different polymorphs, that is, the 2H (trigonal prismatic $D_{3h}$), 1T′ (octahedral $O_h$), and 3R (rhombohedral $C_{3v}^5$) phases.[1] By tuning the arrangement of the S atoms, MoS$_2$ can convert from the semiconducting 2H to the metallic 1T′ phase. Such a rearrangement of S atoms is typically caused by interlayer atomic plane gliding induced by electron donation or the intercalation of small molecules or cations.[2−6] Alkali metal cations, especially Li, are typically used to intercalate between the MoS$_2$ layers to induce the 2H to 1T′ phase conversion.[7] Despite many years of study of lithium-intercalated MoS$_2$ (1T′-Li$_x$MoS$_2$), the 1T′ phase is metastable and can easily change to the 2H phase.[7−9] Furthermore, the quick hydration of Li in aqueous solution makes the stable operation of 1T′-MoS$_2$ under HER conditions challenging.[10−13] Upon Li intercalation, the crystal structure of MoS$_2$ is modified, shown by the emergence of broad diffraction peaks and a distinct red shift of Raman modes.[14] However, previous works have mostly only assumed a 2H to 1T′ phase conversion upon the adequate intercalation of Li ions without

paying further attention to the behavior of adsorbed Li.[14,15] Even though there are several theoretical works in the literature investigating the structural transitions in MoS$_2$ monolayers induced by Li adsorption,[16−18] a systematic experimental study on the effect of Li adsorption is still lacking. Whereas, for instance, trace metal impurities are known to play an active role in determining the electrocatalytic properties of graphene,[19] the role of adsorbed Li in the MoS$_2$-catalyzed HER remains ambiguous.

Since the discovery of 1T′-MoS$_2$, it has emerged as a promising candidate for a broad range of applications, including photocatalysis, supercapacitors, and, in particular, as an electrocatalyst for the hydrogen evolution reaction (HER).[3,20−22] Bulk 2H-MoS$_2$ is a poor HER catalyst because the reaction is limited by the density of active sites, which are concentrated at the layer edges or edge-like defect sites on the (0001) basal planes.[23] Significant research efforts have been

devoted to synthesis strategies that can expose more active (edge) sites to enhance the overall HER performance, for example, nanoparticulate $MoS_2$, nanostructured $MoS_2$, or $MoS_2$ basal planes with sulfur vacancies.[24−26] In contrast with its 2H counterpart, the significant catalytic improvement toward HER of 1T′-$MoS_2$ has been ascribed to the intrinsic activity of its basal planes.[8] Numerous studies have reported the structural change (extensive layer displacement or bond distortion) of 2H-$MoS_2$ to 1T′-$MoS_2$ after Li intercalation, and density functional theory (DFT) modeling suggests that the catalytic improvement of Li-intercalated $MoS_2$ can be attributed to octahedral and distorted $MoS_2$ phases.[13,27−31] Nonetheless, a more direct role of the Li ions, which are inevitably present in 1T′-$MoS_2$, in HER catalysis has never been shown. In most cases, excessive amounts of Li are used to induce the 2H-1T′ structural transformation.[11,15,32] However, considering that the local surface chemistry governs the catalytic performance, both excess Li and Li adsorbed on the catalysts may play a vital role during the catalytic reaction as well.

Here we report a study of the role of Li in the $MoS_2$-catalyzed HER. The influence of Li adsorption on the $MoS_2$ 2H-to-1T′ phase transformation was systematically investigated by X-ray photoelectron (XPS) and extended X-ray absorption fine structure (EXAFS) spectroscopies. With the assistance of in-situ IR spectroscopy with NO as a probe molecule as well as $^7Li$ MAS nuclear magnetic resonance (NMR) spectra, we were able to identify the interaction between Li ions and $MoS_2$. Interestingly, Li-adsorbed 2H-$Li_xMoS_2$ ($0 < x < 0.5$) presents much higher activity than 1T′-$Li_xMoS_2$ ($x \approx 1$ or $2$), which sheds new light on understanding the intrinsic activity of lithiated TMDs. This systematic investigation on the adsorption and promotion effects of Li on $MoS_2$ in the electrocatalytic HER will provide a new platform for designing effective TMD-based catalysts.

We adopt a typical impregnation method to prepare a series of carbon-supported $Li_xMoS_2$ catalysts with a precisely controlled Li content (Figure S1). As indicated in Figure 1a, Li is expected to preferentially adsorb on the surface of $MoS_2$ at low concentrations, whereas at high Li concentrations, the structure undergoes a transformation from 2H- to 1T′-$MoS_2$.[17] HR-TEM images (Figure 1b,c and Figure S2) show that the molybdenum sulfide phase is well distributed across the carbon support, and the influence of particle dispersion upon Li addition on HER activity could be ruled out. Because the catalytic activity of $MoS_2$ is known to be significantly enhanced by edge-terminated surfaces,[24,33,34] we predict here through first-principles (DFT) calculations the surface formation energy of a (0001) monolayer of 1T′-$MoS_2$ with a pristine Mo edge and how it is stabilized through adsorbed Li atoms in increasing concentration ($Li_xMoS_2$). As shown in Figures S3 and S4, Li adsorption on the Mo-edge surface is found to have a stabilizing effect on the monolayer, as reflected in the monotonic decrease in the surface formation energies with increasing adsorbed Li concentration. The stabilization of the Mo-edge monolayers can be rationalized by considering the fact that the adsorption acts to coordinate the Li to the under-coordinated Mo ions, thus providing a closer match to the bulk coordination of the edge species. Moreover, we characterized the electronic structure of $Li_xMoS_2$ by means of X-ray photoelectron spectroscopy (XPS) (Figure 1d,e, Figures S5 and S6, and Tables S4 and S5). The Mo 3d core-level spectra present a shift to lower binding energy for $Li_{1.00}MoS_2$ and $Li_{2.06}MoS_2$ as compared with samples with lower Li loading, indicating the formation of 1T′-$MoS_2$.[3,35,36] Because the S 2p binding energy of 1T′-phase sulfur overlaps with that of
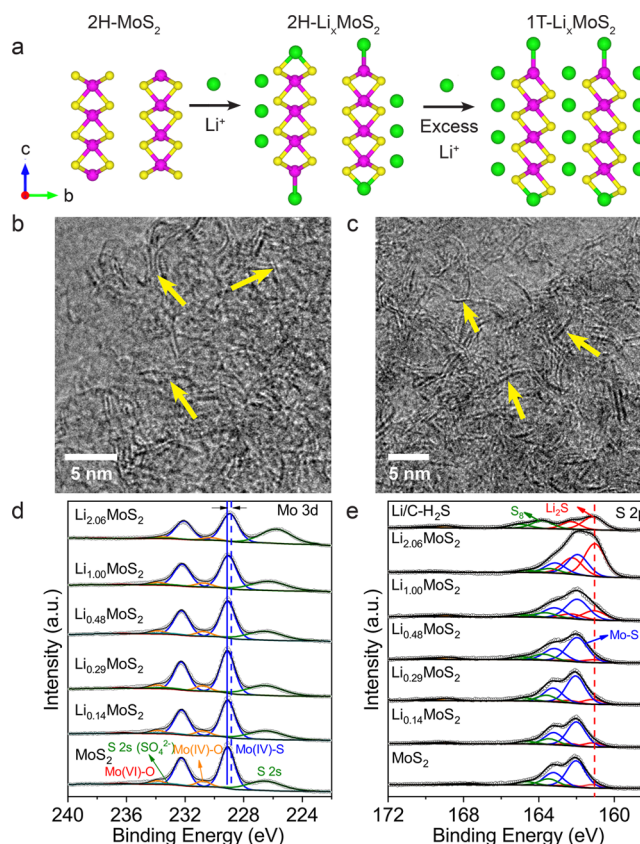


**Figure 1.** (a) Schematic model of 1T′-$Li_xMoS_2$ preparation via Li intercalation. The slab model is periodic in *a* and *b* directions and nonperiodic in *c* direction. (b,c) HR-TEM images of pure $MoS_2$ (b) and $Li_{0.29}MoS_2$ (c) loaded on activated carbon. Yellow arrows indicate $MoS_2$ nanosheets. (d,e) XP spectra of Mo 3d (d) and S 2p (e) for $Li_xMoS_2$/C catalysts with various Li contents.

$Li_2S$,[3,32,33] we cannot quantify the amount of 1T′ phase present based on the S 2p spectra. Consistently, our DFT-calculated core-level binding-energy shifts (Table S5) reveal lower core-level energies of the S 2p and Mo 3d in the $Li_xMoS_2$ monolayers at various Li concentrations compared with the pure 2H-$MoS_2$. In general, the $Li_xMoS_2$ monolayers show lower core-level energies for the S 2p and Mo 3d compared with the pure $MoS_2$ monolayer, with the shifts increasing upon larger Li concentration. The S 2p core-level shifts are in the range of 0.44 to 1.67 eV compared with the Mo 3d core-level shifts in the range of 0.52 to 2.27 eV.

Solid-state $^7Li$ MAS NMR has been used to study the local coordination environments of Li in the $Li_xMoS_2$ samples. As indicated in Figure 2a, the chemical shift at around −7 ppm reveals the interaction between Li and $MoS_2$, which is distinctly different from Li adsorbed on a carbon support (Li/C−He) or mobile $Li_2S$ (Li/C−$H_2S$) species; the latter are presumed not to interact with $MoS_2$. Furthermore, on the basis of a deconvolution of the quantitative NMR spectra (Figures S7 and S8), we have analyzed the composition of the Li species. Table 1 presents different Li component ratios of $Li_xMoS_2$/C, indicating that excess Li exists in the form of $Li_2S$ and Li/C only at high Li concentrations (in samples $Li_{1.00}MoS_2$ and $Li_{2.06}MoS_2$) and Li fully adsorbs on $MoS_2$ at low loading. To gain insight into the proximity between mobile $Li_2S$ and $Li_xMoS_2$, a 2D $^7Li−^7Li$ RFDR (radio-frequency-driven recoupling) MAS NMR experiment was carried out (Figure 2b,c).[37,38]
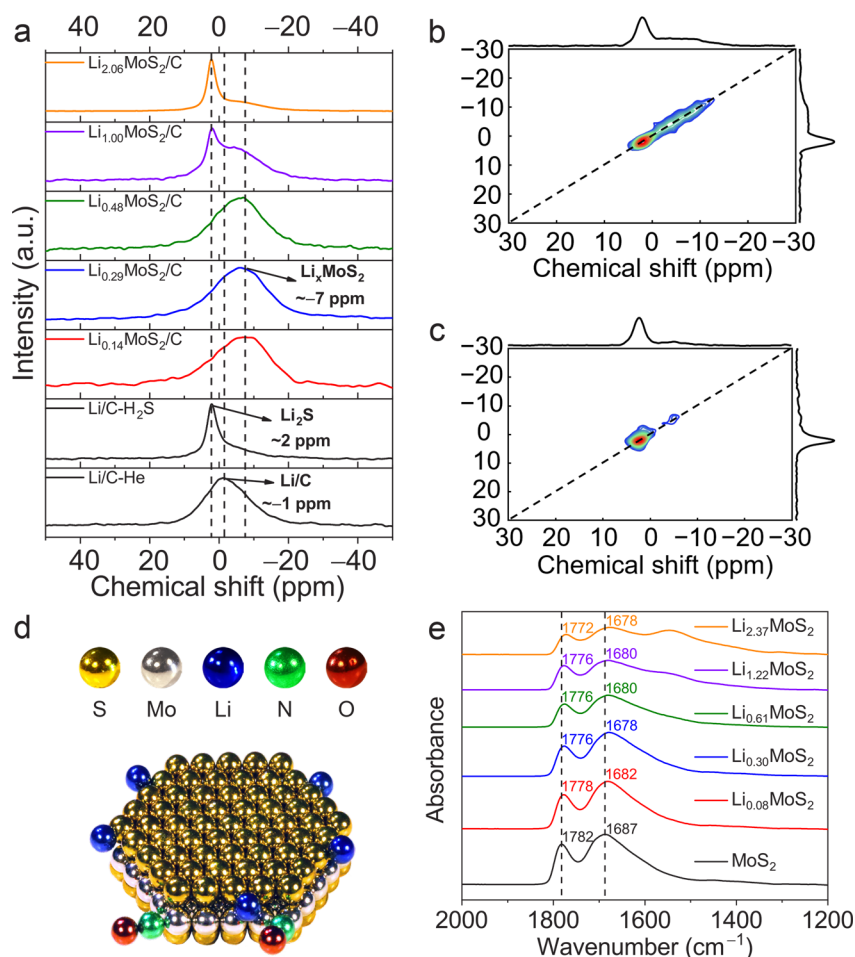
Figure 2. (a) $^7$Li MAS NMR spectra acquired at 20 kHz. Li/C−He and Li/C−H$_2$S represent Li precursor loaded on activated carbon after annealing in He and H$_2$S atmosphere, respectively. (b,c) $^7$Li−$^7$Li RFDR MAS NMR spectra of Li$_{2.06}$MoS$_2$/C with relaxation times of 100 $\mu$s (b) and 1 s (c). (d) Schematic model for the interaction of NO molecules with Li-adsorbed MoS$_2$. (e) IR spectra of a certain amount (0.52 mol$_{NO}$ mol$_{Mo}$$^{-1}$) of NO doses adsorbed on Li$_x$MoS$_2$/Al$_2$O$_3$ with different Li contents.

**Table 1. Summary for the Ratios of Different Li Components Based on Deconvolution of $^7$Li NMR Peaks**

| sample | Li/Mo molar ratio (ICP-OES) | Li$_2$S component area (%) | Li/C component area (%) | Li$_x$MoS$_2$ component area (%) |
|---|---|---|---|---|
| Li$_{0.14}$MoS$_2$ | 0.14 | | | 100 |
| Li$_{0.29}$MoS$_2$ | 0.29 | | | 100 |
| Li$_{0.48}$MoS$_2$ | 0.48 | | | 100 |
| Li$_{1.00}$MoS$_2$ | 1.00 | 18.6 | 25.2 | 56.2 |
| Li$_{2.06}$MoS$_2$ | 2.06 | 47.9 | 17.3 | 34.8 |
| Li/C−H$_2$S | | 41.8 | 58.2 | |
| Li/C−He | | | 100 | |

The absence of cross-peaks indicates that Li ions at different sites are not in close vicinity. Figure 2d,e and Figures S9−S11 display the scheme of NO adsorption on Li$_x$MoS$_2$. A gradual red shift of the IR bands at ∼1782 cm$^{-1}$ (coupled mononitrosyl or dinitrosyl, symmetric stretch, $\nu_s$) and ∼1687 cm$^{-1}$ (coupled mononitrosyl or dinitrosyl, asymmetric stretch, $\nu_{as}$) (Figure 2e and Figure S10) is observed upon the introduction of Li ions.

X-ray absorption spectroscopy (XAS) was conducted to investigate the atomic structural change of Li$_x$MoS$_2$ upon interaction with Li (Figures S12 and S13). The Fourier transforms of the Mo K-edge extended X-ray absorption fine structures (EXAFS) in $R$-space are shown in Figure 3. The

distinct downshift of the Mo−Mo bond from 3.16 to 2.80 Å (Table 2) in Li$_{1.00}$MoS$_2$ and Li$_{2.06}$MoS$_2$ reflects the characteristic length of the Mo−Mo bond in 1T'-MoS$_2$.[10,39,40] Upon Li adsorption or intercalation, Li atoms donate electron density to the d band of 2H-MoS$_2$, thereby transforming it into 1T'-MoS$_2$ with octahedrally coordinated Mo atoms.[17,40] Further insight into the charge transfer of MoS$_2$ after Li adsorption was gained through a Bader charge and differential charge density analysis of monolayer 1T'-MoS$_2$ with different concentrations of adsorbed Li. The calculated Bader charges of S and Mo atoms before and after the adsorption of Li ions (Table S6) indicate that the adsorption process is characterized by a charge transfer from the Li atoms to the S and Mo atoms. Consistently, from the differential charge density isosurface plots in Figure 3g, where the pink and cyan blue contours indicate an electron density increase and decrease by 0.02 e$^-$ Å$^{-3}$, respectively, it is obvious that the electron densities of the Li atoms (cyan contours) were transferred to the S-2p and Mo-3d orbitals (pink contours) in the process of Li adsorption. The electron transfer from the Li atoms to the S and Mo atoms is responsible for the observed distortions in the Mo−S and Mo−Mo bonds of the Li$_x$MoS$_2$ monolayers, as obtained from EXAFS fitting (Table 2) and confirmed by DFT results (Table S7).

The HER performance of different Li$_x$MoS$_2$ catalysts on glassy carbon was evaluated using a standard three-electrode
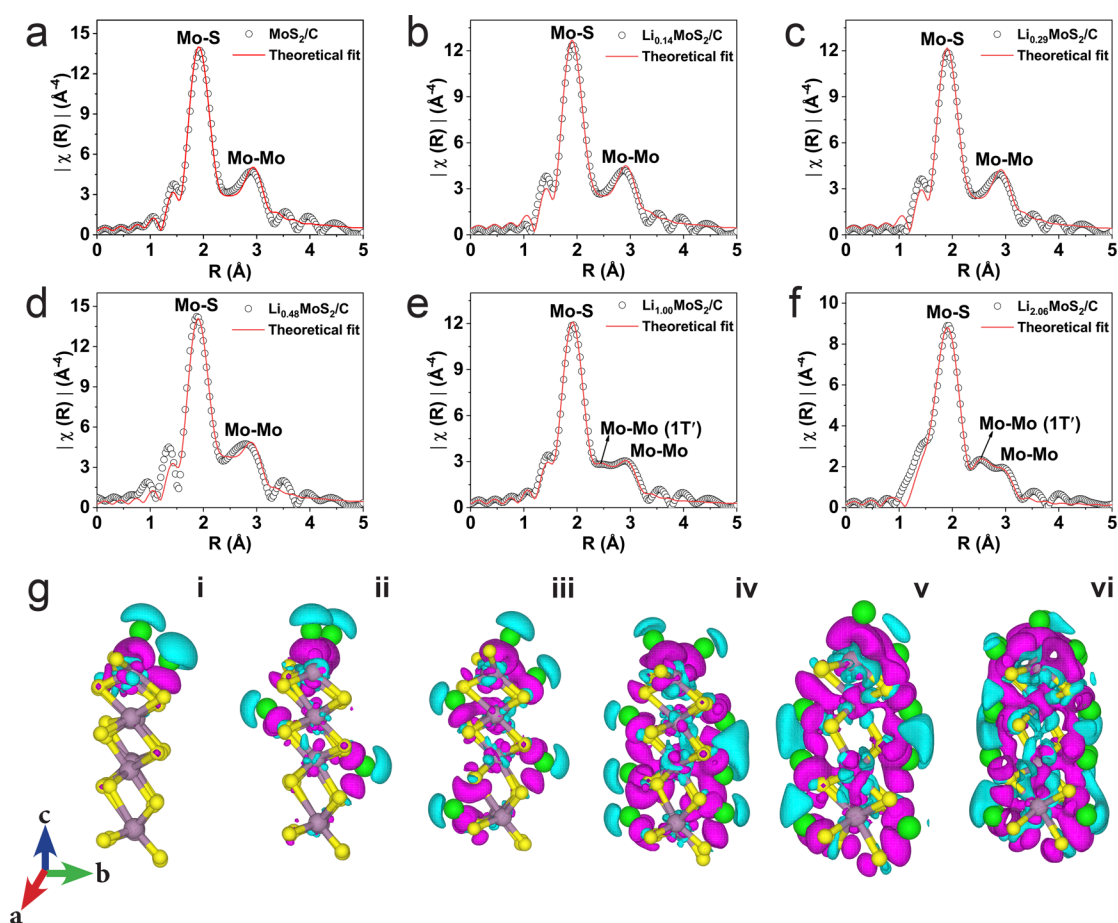
Figure 3. (a−f) Mo K-edge EXAFS spectra plotted as the magnitude of the Fourier transform of $MoS_2$ (a), $Li_{0.14}MoS_2$ (b), $Li_{0.29}MoS_2$ (c), $Li_{0.48}MoS_2$ (d), $Li_{1.00}MoS_2$ (e), and $Li_{2.06}MoS_2$ (f). Open black circles represent experimental data, and red curves are fitted spectra. (g) Electron density difference isosurface contours of $MoS_2$ upon Li adsorption, where the pink and cyan contours indicate an electron density increase and decrease by 0.02 $e^-$ $Å^{-3}$, respectively. (Gray, yellow, and green correspond to Mo, S, and Li atoms, respectively.) i−vi correspond to $Li_{0.13}MoS_2$, $Li_{0.25}MoS_2$, $Li_{0.31}MoS_2$, $Li_{0.5}MoS_2$, $Li_{1.00}MoS_2$, and $Li_{2.00}MoS_2$ respectively.

**Table 2. Mo K-Edge EXAFS Fitting Results of Molybdenum Sulfide Loaded on Carbon Support**

| sample | Mo−S | | | Mo−Mo | | | Mo−Mo (short) | | | $\Delta E_0$ (eV) | R factor |
|---|---|---|---|---|---|---|---|---|---|---|---|
| | CN | R (Å) | $\sigma^2$ | CN | R (Å) | $\sigma^2$ | CN | R (Å) | $\sigma^2$ | | |
| $MoS_2$ | 5.46 ± 0.48 | 2.405 ± 0.006 | 0.003 | 1.93 | 3.157 ± 0.013 | 0.002 | | | | 3.42 | 0.011 |
| $Li_{0.14}MoS_2$ | 4.94 ± 0.54 | 2.408 ± 0.008 | 0.003 | 1.60 | 3.158 ± 0.016 | 0.001 | | | | 1.44 | 0.015 |
| $Li_{0.29}MoS_2$ | 4.80 ± 0.55 | 2.409 ± 0.008 | 0.003 | 1.48 | 3.158 ± 0.017 | 0.001 | | | | 1.00 | 0.017 |
| $Li_{0.48}MoS_2$ | 5.78 ± 0.79 | 2.397 ± 0.010 | 0.004 | 2.35 | 3.152 ± 0.019 | 0.003 | 1.29 ± 1.28 | 2.824 ± 0.082 | 0.010 | 0.83 | 0.017 |
| $Li_{1.00}MoS_2$ | 5.52 ± 0.44 | 2.408 ± 0.006 | 0.005 | 1.43 | 3.166 ± 0.017 | 0.003 | 1.32 ± 0.64 | 2.785 ± 0.038 | 0.010 | 2.43 | 0.005 |
| $Li_{2.06}MoS_2$ | 4.80 ± 1.01 | 2.422 ± 0.016 | 0.006 | 0.99 | 3.176 ± 0.030 | 0.003 | 1.33 ± 0.94 | 2.800 ± 0.058 | 0.010 | 3.82 | 0.012 |

electrochemical configuration in 0.1 M $H_2SO_4$ deaerated with Ar (Figures S14 and S15). The polarization curves (Figure 4a) show that a small amount of Li adsorption ($Li_{0.14}MoS_2$ and $Li_{0.29}MoS_2$) greatly decreases the onset overpotential and improves the current density for HER as compared with pure $MoS_2$. Interestingly, the cathodic current was lower in the case of $Li_{0.48}MoS_2$ and decreased sharply for $Li_{1.00}MoS_2$ and $Li_{2.06}MoS_2$. Tafel slopes in Figure 4b reveal the same trend, that is, that an optimum amount of Li loading dramatically improves the HER activity (lower Tafel slope and higher cathodic current density), whereas an excess of Li hinders the electrocatalytic reaction. To quantify the catalytic activity, we measured the actual number of active sites using the IR NO titration method (for further details see the experimental section of the SI). On the basis of this

method, we have determined the number of active sites to be ~3.0 × $10^{15}$ sites $cm^{-2}$ (based on geometric electrode area; Table S8 and Figures S16 and S17). The turnover frequency (TOF) ($s^{-1}$) of the hydrogen evolution was calculated, as shown in Figure 4c. Among the compared catalysts, $Li_{0.14}MoS_2$ and $Li_{0.29}MoS_2$ show the highest TOF, which is three times larger than that of bare $MoS_2$ at a cathodic overpotential of 300 mV. It is worth noting that despite the presence of the 1T′ phase in $Li_{1.00}MoS_2$ and $Li_{2.06}MoS_2$, the relatively lower catalytic activity of these samples compared with that of $Li_{0.29}MoS_2$ (entirely 2H phase) indicates that next to Li intercalation, Li adsorption plays a key role in describing the high HER activity of $Li_xMoS_2$ electrocatalysts.[28,41−43]
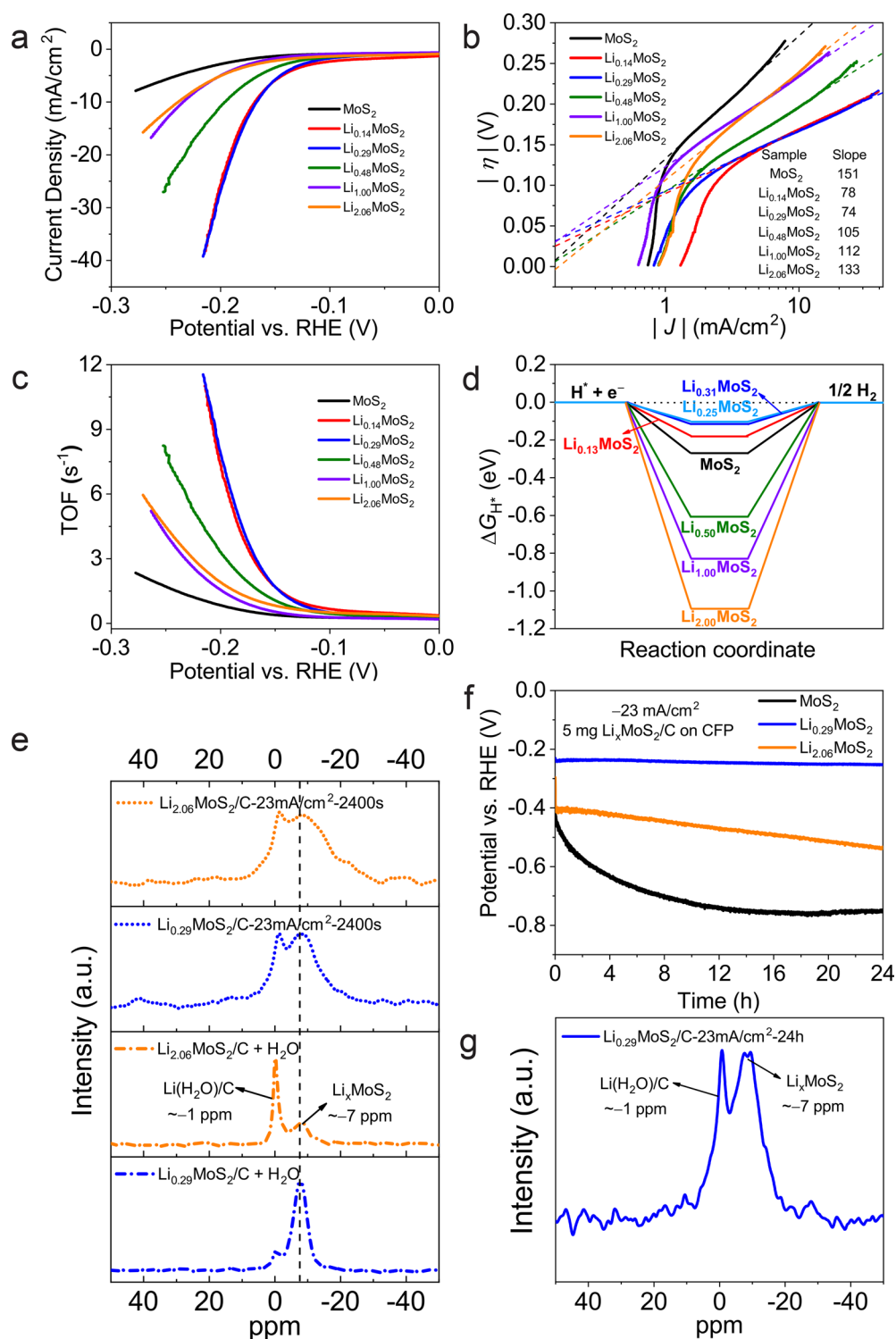
**Figure 4.** (a) Linear sweep voltammetry (LSV) curves (corrected by uncompensated resistance) of Li$_x$MoS$_2$ catalysts on glassy carbon electrode (GCE). (b) Tafel plots (mV/dec) of corresponding catalysts derived from panel a. Solid lines represent experimental data, and dashed lines represent the linear fit. Electrolyte: 0.1 M H$_2$SO$_4$, scan rate: 5 mV/s. (c) Calculated turnover frequency (TOF) as a function of applied potential for Li$_x$MoS$_2$/C catalysts. (d) DFT calculated free Gibbs energy of proton adsorption on Li-adsorbed MoS$_2$ Mo edge. (e) $^7$Li MAS NMR spectrum acquired at 20 kHz for Li$_x$MoS$_2$ catalysts in contact with H$_2$O and after HER. (f) Galvanostatic responses ($E-t$) recorded on MoS$_2$ (black), Li$_{0.29}$MoS$_2$ (blue), and Li$_{2.06}$MoS$_2$ (orange) for 24 h at a constant current density of −23 mA/cm$^2$. (g) $^7$Li MAS NMR spectrum acquired at 20 kHz for Li$_{0.29}$MoS$_2$ catalyst after HER test for 24 h.

To gain further insight into the synergistic effect of Li adsorption on the MoS$_2$-catalyzed HER, we have calculated the Gibbs free energy of hydrogen adsorption ($\Delta G_{H*}$) on Li$_x$MoS$_2$ monolayers, as shown in Figure 4d. The adsorption structures of

hydrogen on the Li$_x$MoS$_2$ monolayers are shown in Figures S19−S22. The value of $\Delta G_{H*}$ must be close to zero, indicating that the free energy of adsorbed H is close to that of the reactant or product.[44,45] Among the various Li$_x$MoS$_2$ samples studied,

$Li_{0.25}MoS_2$ and $Li_{0.31}MoS_2$ compositions show the smallest $|\Delta G_{H*}|$ value of 0.11 and 0.12 eV, respectively, both of which are similar to the $\Delta G_{H*}$ value for the well-known and highly efficient Pt catalyst, that is, $|\Delta G^{Pt}_{H*}| \approx 0.09$ eV. Similarly, the $|\Delta G_{H*}|$ for the $Li_{0.13}MoS_2$ composition was calculated to be 0.16 eV compared with 0.29 eV in $MoS_2$ without Li adsorption. Largely negative $\Delta G_{H*}$ values of −0.60, −0.84, and −1.09 eV were calculated for the $Li_{0.5}MoS_2$, $Li_{1.00}MoS_2$, and $Li_{2.00}MoS_2$ monolayers, respectively, indicating that the chemical adsorption of H* on their Mo edges is too strong, which makes them less active in the HER. We have also considered H adsorption on the S edge of the $Li_xMoS_2$ with increasing Li concentration. As can be seen Figures S21−27, the $\Delta G_{H*}$ values at the pure, $Li_{0.13}MoS_2$, $Li_{0.25}MoS_2$, $Li_{0.31}MoS_2$, $Li_{0.50}MoS_2$, $Li_{1.00}MoS_2$, and $Li_{2.00}MoS_2$ S edges are −0.43, −0.32, −0.34, −0.30, −0.77, −0.92, and −1.32 eV, respectively. Similar to the results obtained at the Mo edge, the stronger chemical adsorption of H* on the S edges with increased Li concentration suggests that higher Li compositions will be less active in HER. However, the more optimum $\Delta G_{H*}$ values predicted at lower Li concentrations at the Mo edge compared with the S edge demonstrate a superior HER activity of the Mo edges. This is consistent with previous theoretical predictions that showed the Mo edges to be more active for HER than S edges.[46,47] Further insights into the adsorption of H on the Mo edge of the $Li_xMoS_2$ materials were gained through a Bader charge and electron density difference isosurface analyses. Consistent with the higher $|\Delta G_{H*}|$, Bader population analyses revealed that the adsorbed H atom on the Mo edge draws larger amounts of charge from the $Li_{0.50}MoS_2$, $Li_{1.00}MoS_2$, and $Li_{2.00}MoS_2$ monolayers, calculated at 0.52, 0.63, and 0.82 e⁻ respectively, compared with 0.29, 0.39, 0.35, and 0.36 e⁻ drawn from the pure $MoS_2$, $Li_{0.13}MoS_2$, $Li_{0.25}MoS_2$, and $Li_{0.31}MoS_2$ monolayers. The analysis of the electron density difference isosurfaces (Figure S24) of H adsorbed at pure and $Li_xMoS_2$ Mo edge reveals electron density accumulation (pink contours) around the centers of the newly formed H−Mo bonds, indicating ionic bonding. The smaller amount of charge gained by adsorbed H atoms from the $Li_{0.13}MoS_2$, $Li_{0.25}MoS_2$, and $Li_{0.31}MoS_2$ monolayers suggests that their hydrogen− surface bonds are neither too strong nor too weak (i.e., $|\Delta G_{H*}| \approx$ 0) to limit the recombination of the adsorbed H atoms to evolve molecular hydrogen via a Volmer−Tafel or Volmer−Heyrovsky mechanism,[48] therefore resulting in the observed increase in HER activity.

As Li can easily hydrolyze in $H_2O$,[49] we have employed $^7Li$ MAS NMR spectroscopy to probe the local coordination environments of Li in the presence of $H_2O$. As shown in Figure 4e, a small portion of Li migrates to the carbon support (chemical shift: around −1 ppm) for $Li_{0.29}MoS_2$ once in contact with $H_2O$, whereas most Li remains adsorbed on $MoS_2$ (chemical shift: ∼−7 ppm). Additionally, and in contrast with $MoS_2$ and $Li_{2.06}MoS_2$, $Li_{0.29}MoS_2$ exhibits outstanding long-term electrochemical stability at −23 mA/cm² with an increase in overpotential of only 10 mV after 24 h (Figure 4f and Figures S18 and S19). The spent $Li_{0.29}MoS_2$ catalyst after 24 h of stability testing was further subjected to an NMR analysis. As shown in Figure 4g, the presence of Li species for $Li_{0.29}MoS_2$ after long-term HER measurements indicates the strong interaction between Li and $MoS_2$, further illustrating the promotion effects of Li adsorption for $MoS_2$-catalyzed HER.

In conclusion, we have systematically employed a suite of complementary experimental and computational techniques to investigate the effect of Li adsorption on the phase conversion and HER activity of $MoS_2$ catalysts. The promoting effect of Li adsorption on 2H-$MoS_2$ in enhancing the electrocatalytic hydrogen evolution was shown for the first time. With the assistance of IR spectroscopy using NO as a probe molecule, we experimentally determined the number of active sites for $Li_xMoS_2$ catalysts, which allowed us to determine the TOF of the catalysts. Both experimental and theoretical results indicate that, next to Li intercalation, Li adsorption plays a key role in describing the high HER activity of $Li_xMoS_2$ electrocatalysts. Whereas Li intercalation causes a phase transition from 2H- to 1T′-$MoS_2$ and, with that, impacts on electronic properties such as conductivity, Li adsorption leads a promotion of the HER active edge sites by changing $\Delta G_{H*}$ in a favorable direction. Thus the overall influence of Li in the $MoS_2$-catalyzed HER appears to be more complex than initially reported. Following these results, we believe that an appropriate amount of adsorbed Li or other alkali cations on TMDs would change their corresponding electron density, resulting in a beneficial tuning of the activity in electrocatalytic reactions involving proton adsorption and reduction.

## ■ ASSOCIATED CONTENT

**Ⓢ Supporting Information**

The Supporting Information is available free of charge on the ACS Publications website at DOI: 10.1021/acsenergy-lett.9b00945.

> Experimental and theoretical details as well as supplementary figures and discussions (PDF)

## ■ AUTHOR INFORMATION

**Corresponding Author**

*E-mail: J.P.Hofmann@tue.nl.

**ORCID** ⓘ

Longfei Wu: 0000-0001-6330-3613
Nelson Y. Dzade: 0000-0001-7733-9473
Miao Yu: 0000-0002-3155-5901
Arno J. F. van Hoof: 0000-0002-9649-031X
Heiner Friedrich: 0000-0003-4582-0064
Nora H. de Leeuw: 0000-0002-8271-0545
Emiel J. M. Hensen: 0000-0002-9754-2417
Jan P. Hofmann: 0000-0002-5765-1096

**Notes**

The authors declare no competing financial interest.

## ■ ACKNOWLEDGMENTS

## ■ REFERENCES

(1) Toh, R. J.; Sofer, Z.; Luxa, J.; Sedmidubský, D.; Pumera, M. 3R Phase of MoS$_2$ and WS$_2$ Outperforms the Corresponding 2H Phase for Hydrogen Evolution. *Chem. Commun.* **2017**, *53*, 3054−3057.

(2) Lin, Y. C.; Dumcenco, D. O.; Huang, Y. S.; Suenaga, K. Atomic Mechanism of The Semiconducting-to-Metallic Phase Transition in Single-Layered MoS$_2$. *Nat. Nanotechnol.* **2014**, *9*, 391−396.

(3) Acerce, M.; Voiry, D.; Chhowalla, M. Metallic 1T Phase MoS$_2$ Nanosheets as Supercapacitor Electrode Materials. *Nat. Nanotechnol.* **2015**, *10*, 313−318.

(4) Lukowski, M. A.; Daniel, A. S.; Meng, F.; Forticaux, A.; Li, L.; Jin, S. Enhanced Hydrogen Evolution Catalysis from Chemically Exfoliated Metallic MoS$_2$ Nanosheets. *J. Am. Chem. Soc.* **2013**, *135*, 10274−10277.

(5) Mahler, B.; Hoepfner, V.; Liao, K.; Ozin, G. A. Colloidal Synthesis of 1T-WS$_2$ and 2H-WS$_2$ Nanosheets: Applications for Photocatalytic Hydrogen Evolution. *J. Am. Chem. Soc.* **2014**, *136*, 14121−14127.

(6) Yin, Y.; Zhang, Y.; Gao, T.; Yao, T.; Zhang, X.; Han, J.; Wang, X.; Zhang, Z.; Xu, P.; Zhang, P.; Cao, X.; Song, B.; Jin, S. Synergistic Phase and Disorder Engineering in 1T-MoSe$_2$ Nanosheets for Enhanced Hydrogen-Evolution Reaction. *Adv. Mater.* **2017**, *29*, 1700311.

(7) Attanayake, N. H.; Thenuwara, A. C.; Patra, A.; Aulin, Y. V.; Tran, T. M.; Chakraborty, H.; Borguet, E.; Klein, M. L.; Perdew, J. P.; Strongin, D. R. Effect of Intercalated Metals on the Electrocatalytic Activity of 1T-MoS$_2$ for the Hydrogen Evolution Reaction. *ACS Energy Lett.* **2018**, *3*, 7−13.

(8) Tang, Q.; Jiang, D.-e. Mechanism of Hydrogen Evolution Reaction on 1T-MoS$_2$ from First Principles. *ACS Catal.* **2016**, *6*, 4953−4961.

(9) Maitra, U.; Gupta, U.; De, M.; Datta, R.; Govindaraj, A.; Rao, C. N. Highly Effective Visible-light-induced H$_2$ Generation by Single-layer 1T-MoS$_2$ and A Nanocomposite of Few-layer 2H-MoS$_2$ with Heavily Nitrogenated Graphene. *Angew. Chem., Int. Ed.* **2013**, *52*, 13057−13061.

(10) Chen, Z.; Leng, K.; Zhao, X.; Malkhandi, S.; Tang, W.; Tian, B.; Dong, L.; Zheng, L.; Lin, M.; Yeo, B. S.; Loh, K. P. Interface Confined Hydrogen Evolution Reaction in Zero Valent Metal Nanoparticles-intercalated Molybdenum Disulfide. *Nat. Commun.* **2017**, *8*, 14548.

(11) Leng, K.; Chen, Z.; Zhao, X.; Tang, W.; Tian, B.; Nai, C. T.; Zhou, W.; Loh, K. P. Phase Restructuring in Transition Metal Dichalcogenides for Highly Stable Energy Storage. *ACS Nano* **2016**, *10*, 9208−9215.

(12) Yu, Y.; Nam, G. H.; He, Q.; Wu, X. J.; Zhang, K.; Yang, Z.; Chen, J.; Ma, Q.; Zhao, M.; Liu, Z.; et al. High Phase-purity 1T'-MoS$_2$- and 1T'-MoSe$_2$-layered Crystals. *Nat. Chem.* **2018**, *10*, 638−643.

(13) Voiry, D.; Yamaguchi, H.; Li, J.; Silva, R.; Alves, D. C. B.; Fujita, T.; Chen, M.; Asefa, T.; Shenoy, V. B.; Eda, G.; Chhowalla, M. Enhanced Catalytic Activity in Strained Chemically Exfoliated WS$_2$ Nanosheets for Hydrogen Evolution. *Nat. Mater.* **2013**, *12*, 850−855.

(14) Tan, S. J. R.; Sarkar, S.; Zhao, X.; Luo, X.; Luo, Y. Z.; Poh, S. M.; Abdelwahab, I.; Zhou, W.; Venkatesan, T.; Chen, W.; Quek, S. Y.; Loh, K. P. Temperature- and Phase-Dependent Phonon Renormalization in 1T'-MoS$_2$. *ACS Nano* **2018**, *12*, 5051−5058.

(15) Chang, K.; Hai, X.; Pang, H.; Zhang, H.; Shi, L.; Liu, G.; Liu, H.; Zhao, G.; Li, M.; Ye, J. Targeted Synthesis of 2H- and 1T-Phase MoS$_2$ Monolayers for Catalytic Hydrogen Evolution. *Adv. Mater.* **2016**, *28*, 10033−10041.

(16) Zheng, Y.; Huang, Y.; Shu, H.; Zhou, X.; Ding, J.; Chen, X.; Lu, W. The Effect of Lithium Adsorption on the Formation of 1T-MoS$_2$ Phase Based on First-principles Calculation. *Phys. Lett. A* **2016**, *380*, 1767−1771.

(17) Nasr Esfahani, D.; Leenaerts, O.; Sahin, H.; Partoens, B.; Peeters, F. M. Structural Transitions in Monolayer MoS$_2$ by Lithium Adsorption. *J. Phys. Chem. C* **2015**, *119*, 10602−10609.

(18) Ersan, F.; Gökoğlu, G.; Aktürk, E. Adsorption and Diffusion of Lithium on Monolayer Transition Metal Dichalcogenides (MoS$_{2(1−x)}$Se$_{2x}$) Alloys. *J. Phys. Chem. C* **2015**, *119*, 28648−28653.

(19) Wang, L.; Ambrosi, A.; Pumera, M. "Metal-free" Catalytic Oxygen Reduction Reaction on Heteroatom- Doped Graphene is Caused by Trace Metal Impurities. *Angew. Chem., Int. Ed.* **2013**, *52*, 13818−13821.

(20) Bai, S.; Wang, L.; Chen, X.; Du, J.; Xiong, Y. Chemically Exfoliated Metallic MoS$_2$ Nanosheets: A Promising Supporting Co-catalyst for Enhancing the Photocatalytic Performance of TiO$_2$ Nanocrystals. *Nano Res.* **2015**, *8*, 175−183.

(21) Geng, X.; Sun, W.; Wu, W.; Chen, B.; Al-Hilo, A.; Benamara, M.; Zhu, H.; Watanabe, F.; Cui, J.; Chen, T. P. Pure and Stable Metallic Phase Molybdenum Disulfide Nanosheets for Hydrogen Evolution Reaction. *Nat. Commun.* **2016**, *7*, 10672.

(22) Cordova, A.; Blanchard, P.; Lancelot, C.; Frémy, G.; Lamonier, C. Probing the Nature of the Active Phase of Molybdenum-Supported Catalysts for the Direct Synthesis of Methylmercaptan from Syngas and H$_2$S. *ACS Catal.* **2015**, *5*, 2966−2981.

(23) Velický, M.; Toth, P. S. From Two-dimensional Materials to Their Heterostructures: An Electrochemist's Perspective. *Applied Materials Today* **2017**, *8*, 68−103.

(24) Jaramillo, T. F.; Jørgensen, K. P.; Bonde, J.; Nielsen, J. H.; Horch, S.; Chorkendorff, I. Identification of Active Edge Sites for Electro-chemical H$_2$ Evolution from MoS$_2$ Nanocatalysts. *Science* **2007**, *317*, 100−102.

(25) Seo, B.; Jung, G. Y.; Sa, Y. J.; Jeong, H. Y.; Cheon, J. Y.; Lee, J. H.; Kim, H. Y.; Kim, J. C.; Shin, H. S.; Kwak, S. K.; Joo, S. H. Monolayer-precision Synthesis of Molybdenum Sulfide Nanoparticles and Their Nanoscale Size Effects in the Hydrogen Evolution Reaction. *ACS Nano* **2015**, *9*, 3728−3739.

(26) Tsai, C.; Li, H.; Park, S.; Park, J.; Han, H. S.; Nørskov, J. K.; Zheng, X.; Abild-Pedersen, F. Electrochemical Generation of Sulfur Vacancies in the Basal Plane of MoS$_2$ for Hydrogen Evolution. *Nat. Commun.* **2017**, *8*, 15113.

(27) Chou, S. S.; Sai, N.; Lu, P.; Coker, E. N.; Liu, S.; Artyushkova, K.; Luk, T. S.; Kaehr, B.; Brinker, C. J. Understanding Catalysis in a Multiphasic Two-dimensional Transition Metal Dichalcogenide. *Nat. Commun.* **2015**, *6*, 8311.

(28) Voiry, D.; Salehi, M.; Silva, R.; Fujita, T.; Chen, M.; Asefa, T.; Shenoy, V. B.; Eda, G.; Chhowalla, M. Conducting MoS$_2$ Nanosheets as Catalysts for Hydrogen Evolution Reaction. *Nano Lett.* **2013**, *13*, 6222−6227.

(29) Asadi, M.; Kumar, B.; Behranginia, A.; Rosen, B. A.; Baskin, A.; Repnin, N.; Pisasale, D.; Phillips, P.; Zhu, W.; Haasch, R.; Klie, R. F.; Kral, P.; Abiade, J.; Salehi-Khojin, A. Robust Carbon Dioxide Reduction on Molybdenum Disulphide Edges. *Nat. Commun.* **2014**, *5*, 4470.

(30) Kappera, R.; Voiry, D.; Yalcin, S. E.; Branch, B.; Gupta, G.; Mohite, A. D.; Chhowalla, M. Phase-engineered Low-resistance Contacts for Ultrathin MoS$_2$ Transistors. *Nat. Mater.* **2014**, *13*, 1128.

(31) Luxa, J.; Vosecký, P.; Mazánek, V.; Sedmidubský, D.; Pumera, M.; Sofer, Z. Cation-Controlled Electrocatalytical Activity of Transition-Metal Disulfides. *ACS Catal.* **2018**, *8*, 2774−2781.

(32) Zheng, J.; Zhang, H.; Dong, S.; Liu, Y.; Tai Nai, C.; Suk Shin, H.; Young Jeong, H.; Liu, B.; Ping Loh, K. High Yield Exfoliation of Two-dimensional Chalcogenides Using Sodium Naphthalenide. *Nat. Commun.* **2014**, *5*, 2995.

(33) Gao, M. R.; Chan, M. K.; Sun, Y. Edge-terminated Molybdenum Disulfide with a 9.4-Å Interlayer Spacing for Electrochemical Hydrogen Production. *Nat. Commun.* **2015**, *6*, 7493.

(34) Zhao, X.; Fu, D.; Ding, Z.; Zhang, Y. Y.; Wan, D.; Tan, S. J. R.; Chen, Z.; Leng, K.; Dan, J.; Fu, W.; Geng, D.; Song, P.; Du, Y.; Venkatesan, T.; Pantelides, S. T.; Pennycook, S. J.; Zhou, W.; Loh, K. P. Mo-Terminated Edge Reconstructions in Nanoporous Molybdenum Disulfide Film. *Nano Lett.* **2018**, *18*, 482−490.

(35) Eda, G.; Yamaguchi, H.; Voiry, D.; Fujita, T.; Chen, M.; Chhowalla, M. Photoluminescence from Chemically Exfoliated MoS$_2$. *Nano Lett.* **2011**, *11*, 5111−5116.

(36) Papageorgopoulos, C. A.; Jaegermann, W. Li intercalation Across and Along the van der Waals Surfaces of MoS$_2$ (0001). *Surf. Sci.* **1995**, *338*, 83−93.

(37) Ogata, K.; Salager, E.; Kerr, C. J.; Fraser, A. E.; Ducati, C.; Morris, A. J.; Hofmann, S.; Grey, C. P. Revealing Lithium-silicide Phase Transformations in Nano-structured Silicon-based Lithium Ion Batteries via in situ NMR Spectroscopy. *Nat. Commun.* **2014**, *5*, 3217.

(38) Bhattacharyya, R.; Key, B.; Chen, H.; Best, A. S.; Hollenkamp, A. F.; Grey, C. P. In Situ NMR Observation of the Formation of Metallic Lithium Microstructures in Lithium Batteries. *Nat. Mater.* **2010**, *9*, 504−510.

(39) Li, H.; Chen, S.; Zhang, Y.; Zhang, Q.; Jia, X.; Zhang, Q.; Gu, L.; Sun, X.; Song, L.; Wang, X. Systematic Design of Superaerophobic Nanotube-array Electrode Comprised of Transition-metal Sulfides for Overall Water Splitting. *Nat. Commun.* **2018**, *9*, 2452.

(40) Dungey, K. E.; Curtis, M. D.; Penner-Hahn, J. E. Structural Characterization and Thermal Stability of MoS$_2$ Intercalation Compounds. *Chem. Mater.* **1998**, *10*, 2152−2161.

(41) Wang, H.; Lu, Z.; Xu, S.; Kong, D.; Cha, J. J.; Zheng, G.; Hsu, P. C.; Yan, K.; Bradshaw, D.; Prinz, F. B.; Cui, Y. Electrochemical Tuning of Vertically Aligned MoS$_2$ Nanofilms and Its Application in Improving Hydrogen Evolution Reaction. *Proc. Natl. Acad. Sci. U. S. A.* **2013**, *110*, 19701−19706.

(42) Lukowski, M. A.; Daniel, A. S.; English, C. R.; Meng, F.; Forticaux, A.; Hamers, R. J.; Jin, S. Highly Active Hydrogen Evolution Catalysis from Metallic WS$_2$ Nanosheets. *Energy Environ. Sci.* **2014**, *7*, 2608−2613.

(43) Ambrosi, A.; Sofer, Z.; Pumera, M. 2H → 1T phase Transition and Hydrogen Evolution Activity of MoS$_2$, MoSe$_2$, WS$_2$ and WSe$_2$ Strongly Depends on the MX$_2$ Composition. *Chem. Commun.* **2015**, *51*, 8450−8453.

(44) Nørskov, J. K.; Bligaard, T.; Logadottir, A.; Kitchin, J. R.; Chen, J. G.; Pandelov, S.; Stimming, U. Trends in the Exchange Current for Hydrogen Evolution. *J. Electrochem. Soc.* **2005**, *152*, J23−J26.

(45) Greeley, J.; Jaramillo, T. F.; Bonde, J.; Chorkendorff, I.; Nørskov, J. K. Computational High-Throughput Screening of Electrocatalytic Materials for Hydrogen Evolution. *Nat. Mater.* **2006**, *5*, 909−913.

(46) Wang, H.; Tsai, C.; Kong, D.; Chan, K.; Abild-Pedersen, F.; Nørskov, J. K.; Cui, Y. Transition-Metal Doped Edge Sites in Vertically Aligned MoS$_2$ Catalysts for Enhanced Hydrogen Evolution. *Nano Res.* **2015**, *8*, 566−575.

(47) Rosen, A. S.; Notestein, J. M.; Snurr, R. Q. Comprehensive Phase Diagrams of MoS$_2$ Edge Sites Using Dispersion-Corrected DFT Free Energy Calculations. *J. Phys. Chem. C* **2018**, *122*, 15318−15329.

(48) Jiao, Y.; Zheng, Y.; Jaroniec, M.; Qiao, S. Z. Design of Electrocatalysts for Oxygen- and Hydrogen-involving Energy Conversion Reactions. *Chem. Soc. Rev.* **2015**, *44*, 2060−2086.

(49) Heising, J.; Kanatzidis, M. G. Exfoliated and Restacked MoS$_2$ and WS$_2$: Ionic or Neutral Species? Encapsulation and Ordering of Hard Electropositive Cations. *J. Am. Chem. Soc.* **1999**, *121*, 11720−11732.